Whistler-mode waves in Mercury's magnetosphere observed by BepiColombo/Mio

Mitsunori Ozaki, Satoshi Yagitani, Yasumasa Kasaba, Yoshiya Kasahara, Shoya Matsuda, Yoshiharu Omura, Mitsuru Hikishima, Fouad Sahraoui, Laurent Mirioni, Gérard Chanteur, et al.

Whistler-mode waves in Mercury's magnetosphere observed by BepiColombo/Mio

Mitsunori Ozaki, Satoshi Yagitani, Yasumasa Kasaba, Yoshiya Kasahara, Shoya Matsuda, Yoshiharu Omura, Mitsuru Hikishima, Fouad Sahraoui, Laurent Mirioni, Gérard Chanteur, et al.

Title (< 90 characters)

Direct evidence of whistler-mode waves in Mercury's magnetosphere: BepiColombo Mio flybys

Authors

Mitsunori Ozaki[1], Satoshi Yagitani[1], Yasumasa Kasaba[2], Yoshiya Kasahara[1], Shoya Matsuda[1], Yoshiharu Omura[3], Mitsuru Hikishima[4], Fouad Sahraoui[5], Laurent Mirioni[5], Gérard Chanteur[5], Satoshi Kurita[3], Satoru Nakazawa[6], Go Murakami[6]

Affiliations

1 Graduate School of Natural Science and Technology, Kanazawa University, Kanazawa, Japan.

2 Graduate School of Science, Tohoku University, Sendai, Japan.

3 Research Institute for Sustainable Humanosphere, Kyoto University, Uji, Japan.

4 Magnedesign Corporation, Nagoya, Japan.

5 Laboratoire de Physique des Plasmas, CNRS - Ecole Polytechnique - Sorbonne Université - Université Paris-Saclay - Observatoire de Paris-Meudon, Palaiseau, France.

6 Institute of Space and Astronautical Science, Japan Aerospace Exploration Agency, Sagamihara, Japan.

Corresponding author

Correspondence to Mitsunori Ozaki

ozaki@is.t.kanazawa-u.ac.jp

Abstract (< 150 words)

Whistler-mode chorus waves are natural electromagnetic emissions known to play a key role in electron acceleration and loss mechanisms via wave–particle interactions in planetary magnetospheres. No evidence of the presence of chorus waves in Mercury's magnetosphere has been reported, because of its small size largely occupied by the planet. Here we present the direct probing of chorus waves in the localized dawn sector during the first and second Mercury flybys by the BepiColombo/Mio spacecraft. Mio's search coil magnetometers detected chorus events with tens of pico-Tesla intensities in the dawn sector, while no clear chorus activity was observed in the night sector. Simulation results suggest that this regional difference could be due to the impact of background magnetic field inhomogeneities on the nonlinear wave generation process. This observational evidence is crucial for understanding the energetic electron dynamics of the localized dawn sector of Mercury's magnetosphere and the diversity of planetary magnetospheres.

Introduction

The planets in our solar system are very diverse[1], with some of them being magnetized (and thus possessing a magnetosphere) while others are not, and some bearing an atmosphere while others do not. This significantly impacts their interactions with the solar wind, a permanent super-Alfvénic and super-sonic plasma flow emitted by the Sun[2]. Understanding the differences between the Solar System planets is extremely important for identifying potentially habitable exoplanets where life can exist. The Earth's magnetosphere acts as an impenetrable barrier for relativistic electrons, protecting lifeforms from direct exposure to such high-energy particles[3]. Although Mercury and Earth are magnetized planets, they exhibit certain differences. Mercury does not hold a rich atmosphere[4], as Earth does, and has weak (approximately 1% of the Earth's) internal magnetic fields that form only a small magnetosphere, as discovered by the Mariner 10 flyby observation in 1974[5]. Electron observations by Mariner 10 showed Earth-like interactions with the solar wind that develop a bow shock and a magnetosheath surrounding Mercury's magnetosphere similar to the morphology of Earth's, but with different spatial and temporal scales[6]. The MESSENGER observations during its flybys in the 2000s and in orbit in the 2010s quantified behaviors (e.g., an axially aligned dipole offset to the north by $0.2R_M$, where R_M is the radius of Mercury) of internal magnetic fields[7, 8, 9] and a small magnetosphere. The MESSENGER's Fast Imaging Plasma Sensor (FIPS) detected ions with energies of 0.1–13 keV, and identified quasi-trapped ring current ions in the planet's magnetosphere[10], but the instrument did not measure electrons. The MESSENGER electron measurements from ~10 keV to several 100 keV were made either directly (e.g., solid state detectors) and/or indirectly using effects such as X-ray fluorescence stimulated in anti-coincidence shields or within the structure of other instruments[11]. The MESSENGER electron observations revealed energetic electrons at all longitudes with energies

ranging from a few up to hundreds of keV, but those electrons have an asymmetric dawn to dusk distribution[11, 12]. The presence of supra-thermal electrons in 1 to 10 keV, inferred from X-ray data and keV-electron precipitation events, were concentrated at the dawn sector of Mercury[13, 14]. MESSENGER also observed "loading and unloading" of the tail magnetic field strength similar to what is observed during substorms on Earth, but with shorter temporal (only a few minutes) scales[15]. The MESSENGER data further showed that ~25% of the dipolarization events in the near-tail were closely correlated with energetic electron injections[16]. Furthermore, those energetic particle injections and dipolarization events are most frequent over the dawn side of the magnetosphere (see a review article[15] and references therein). The planetary loss cone is large and it is not favorable to keep stable particle trapping, because Mercury itself occupies a large portion of the small magnetosphere. However, Mariner 10's and MESSENGER's observations suggest that Mercury's magnetosphere evolves with various dynamical kinetic processes.

It is widely accepted that whistler-mode chorus waves[17, 18], which are natural electromagnetic wave emissions in the very low frequency range (VLF) (several hundreds to tens of kHz), play an important role in electron acceleration and loss around magnetized planets via wave–particle interactions[19, 20, 21, 22]. In particular, chorus waves interact with energetic electrons via cyclotron resonance, which can lead to a localized enhancement of relativistic electrons that form the Earth's and other planetary (Jupiter and Saturn) radiation belts[19, 20, 21, 22, 23, 24]. Chorus waves are commonly observed in the Earth's and other planetary (Jupiter, Saturn, and Uranus) magnetospheres[25], but have not been identified in Mercury's magnetosphere. The Mariner 10 and MESSENGER spacecraft were not equipped with wave instruments that could probe into the VLF range of chorus waves. The BepiColombo/Mio (another name for the Mercury Magnetospheric Orbiter (MMO)) spacecraft that was launched on 20th October 2018[26, 27] fills this gap by carrying a full set of plasma and wave instruments[28, 29], which will allow us to probe the dynamics of the Hermean environment over a broad range of timescales. In particular, the search coil magnetometers on board Mio[30] were carefully designed for probing high-frequency magnetic fluctuations at 0.1 Hz–640 kHz, which include whistler-mode chorus waves, despite the harsh temperature environment that varies from $+200$°C at Mercury's orbit to -55°C during the cruise. To take advantage of the planned Mercury flybys during the cruise phase, the Mio search coil magnetometers were operated to tentatively detect VLF magnetic fields before the instruments are operated with their full capabilities after the final insertion at Mercury and boom deployment. Below, we show that this attempt proved to be conclusive since the Mercury flyby observations gave evidence of chorus waves based on the wave spectrum measured onboard, although finer structures of typical rising-tone elements in the time domain could not be acquired due to the telemetry limitations.

Results

Wave observations by Mio during Mercury flybys

Mio is in a cruise phase and will reach its final orbit around Mercury in December 2025, when all instruments will be deployed and full observations of plasma waves and plasma particles in the magnetosphere will be possible. Nevertheless, there are several other opportunities for measuring plasma waves, such as during planetary flybys. We present wave magnetic field data for the 1st and 2nd Mercury flybys in the VLF range measured by the Mio search coil magnetometers of the plasma wave instruments (PWI)[29] (see Wave magnetic field measurements in Methods section).

Figure 1 shows the Mio orbits and the wave spectra for the 1st (1st October 2021) and 2nd (23rd June 2022) Mercury flyby events, in which the spacecraft crossed the nightside magnetospheric tail toward the dayside region. The orbit is drawn in the Mercury solar magnetospheric (MSM) coordinate system, where $+X$ is oriented sunward, $+Y$ is directed toward dusk perpendicular to the Mercury–Sun line, $+Z$ is oriented parallel to the north magnetic pole, and the origin is the magnetic dipole of Mercury located northward with an offset of 0.2 R_M from the planet center. The closest approaches are at altitude of approximately 200 km at 23:34 UT and 09:44 UT in the 1st and 2nd flybys, respectively. The raw wave spectra include some electromagnetic interference from the spacecraft body (see Figure S1 in Supplementary Information (SI)) because the 5-m MAST boom on which the search coil sensors are mounted is not deployed during the cruise phase. However, whistler-mode waves below the electron cyclotron frequency (estimated from an empirical model[9]) were clearly observed in the frequency range 0.6–2 kHz during the 1st flyby event (23:37 to 23:39 UT). Other wave activity below 1 kHz was observed from 23:20 to 23:22 UT when Mio crossed the magnetic equator (and during 23:29 to 23:31 UT), but it is difficult to determine whether they are natural wave emissions or electromagnetic interference from the spacecraft because of their low signal-to-noise ratio (SNR). Similarly, whistler-mode waves were observed in the frequency range 0.6–1.8 kHz during the 2nd flyby event (09:45 to 09:51 UT). Note that other broadband plasma waves were also observed above 10 kHz, when Mio crossed the dayside magnetopause at 23:42 UT (1st flyby) and 09:50 UT (2nd flyby) and the boundary between the closed and open field lines of the magnetospheric tail in the nightside at 23:19 UT (1st flyby). The frequency of these broadband waves (that extend from ~10 to over 20 kHz, not shown) is higher than the electron cyclotron frequency and possibly lower than the plasma frequency, and may play an important role in locally heating the particles at these boundary layers.

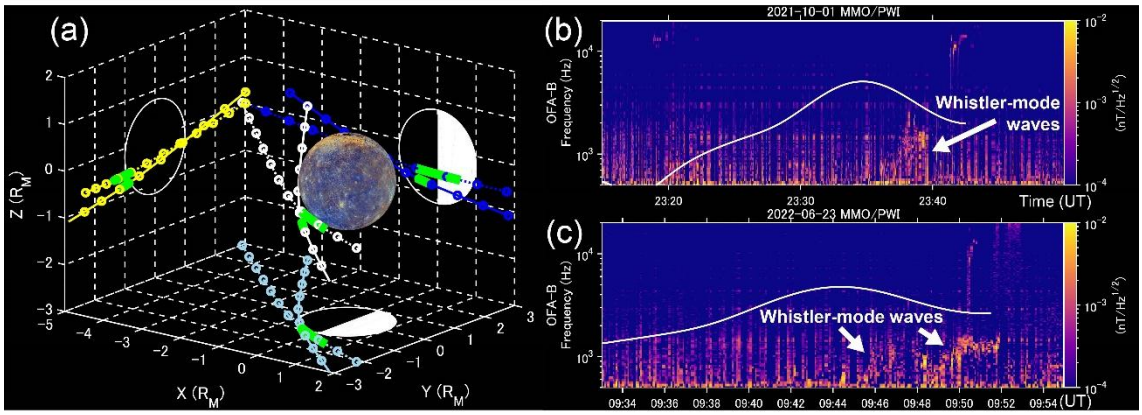

Figure 1. Wave magnetic field spectra of whistler-mode waves in Mercury flybys. (a) BepiColombo Mio orbits. The white solid-dotted line is the Mio trajectory during the 1st flyby (23:10–23:50 UT) and the white dotted line is that for the 2nd flyby (09:10–10:00 UT). The blue, yellow, and sky-blue curves are projections onto the corresponding planes. The dots indicate the Mio location every 5 minutes. The green shaded zone highlights the regions where the whistler-mode waves were observed. (b and c) Wave spectra from 0.5 to 20 kHz measured by the search coil magnetometer during the 1st and 2nd flybys. The white solid lines indicate the electron gyrofrequency estimated from an empirical closed field lines model[9]. Note that panels b and c have different time ranges. The color map image of Mercury in panel (a) is published at https://photojournal.jpl.nasa.gov/catalog/PIA17386. Image credit of Mercury: NASA/Johns Hopkins University Applied Physics Laboratory/Carnegie Institution of Washington.

For both Mercury flyby events, clear whistler-mode wave activity appeared in the dawn side after the closest approach, even for electron cyclotron frequencies of only a few kHz in the nightside. In the 2nd flyby, which showed more activity, the whistler-mode waves were detected up to near the dayside magnetopause. A video showing the spacecraft orbit and the location of the magnetopause and bow shock boundaries is given in the SI (supplementary movies 1 and 2). Because Earth's magnetic moment points southward, the Earth's chorus emission waves also show stronger wave activity in the dawn side[31, 32] due to electron injections from the magnetotail that drift eastward. Mercury's magnetic fields with highly compressed (dayside) and stretched (nightside) structures should impact the wave growth rate (see Figure 2 and the discussion below). Although chorus wave spectra in the Earth's magnetosphere typically show a power gap at half the electron gyrofrequency[33, 34, 35], the observed whistler-mode waves at Mercury do not show such a gap. The reason might be related to the characteristics of wave normal angles at the Mio's off-equatorial region. A power gap can be caused by damping of obliquely propagating waves away from the source region[34]. Unfortunately, information on wave normal angles and polarization is not available

because of telemetry limitation, but this gap should be filled by future flybys that will cover higher latitude regions.

The propagation distance from the source to the spacecraft location may be different between the night and dawn sides. Figure 1a shows that both flyby paths in the nightside were located near the lower magnetic latitudes. This implies that the propagation effects from the source cannot explain the presence of localized whistler-mode waves, and that other physical conditions that impact the wave generation and growth processes are at work. We focus on the difference in the background magnetic field between the night and dawn sectors. Because of the single-point observations, it is difficult to specify regions that grow while propagating from the source region. As a simple assumption, we considered the curvature around a region with B_{min}, which maximizes the linear growth rate[36]. Figure 2 shows the distance between Mio and Mercury, the wave magnetic field intensity, and the curvature of the background magnetic field line for both flyby events. The curvature of the background magnetic field line is calculated from the relation

$$a = \frac{1}{s^2}\left(\frac{B(s)}{B_{min}} - 1\right), \quad (1)$$

where s is an infinitesimal distance along a background magnetic field line from the minimum background magnetic field B_{min} plane with a simple assumption of a parabolic curve[37]. We use $s = 0.2\mathrm{R_M}$ for the wave growth due to magnetic inhomogeneity. The background magnetic field lines are plotted in Supplementary Figure S2 for reference. We found that whistler-mode waves can be generated in a region with a lower curvature (below 1.5×10^{-12} $\mathrm{m^{-2}}$) on the dayside compared with the wave activity measured at the same distance from Mercury in the nightside. The magnetic inhomogeneity is an important parameter that controls the threshold amplitude of the nonlinear wave growth rate for the chorus emission waves[38, 39]. Previous electron observation[12] and simulation[40, 41] studies indicate that moderate energy (keV) electrons can be quasi-trapped at distances ranging from 1.1 to 1.5 $\mathrm{R_M}$. The fact that Mio observed an enhancement of whistler-mode wave activity of several tens of pT for distances of 1.1 to 1.5 $\mathrm{R_M}$ is consistent with the region containing quasi-trapped moderate energy (1–10 keV) electrons[40, 41], as these[6, 11, 16, 40, 41] can act as seed electrons that feed the instability leading to the observed whistler-mode waves. The observed whistler-mode waves should become chorus emission waves at Mercury via a nonlinear wave growth process related to the magnetic inhomogeneity[42]. Assuming an electron density of 10 to 20 $\mathrm{cm^{-3}}$ in the plasma sheet[6, 43], the resonant electron energy for whistler-mode waves[44] at $0.2f_{\mathrm{ce}}$ becomes 60 to 10 keV in both events. The resonant electrons can then precipitate to Mercury's surface, which in turn can cause the X-ray aurora observed at Mercury[13, 14]. Our observations of dawn whistler-mode waves support the MESSENGER observations of localized high-energy electrons concentrated at the dawn side[12] near the equatorial region. The observed dawn whistler-mode waves reported here should also explain (at least partly) the precipitation of keV-energy electrons in the dawn sector[13, 14].

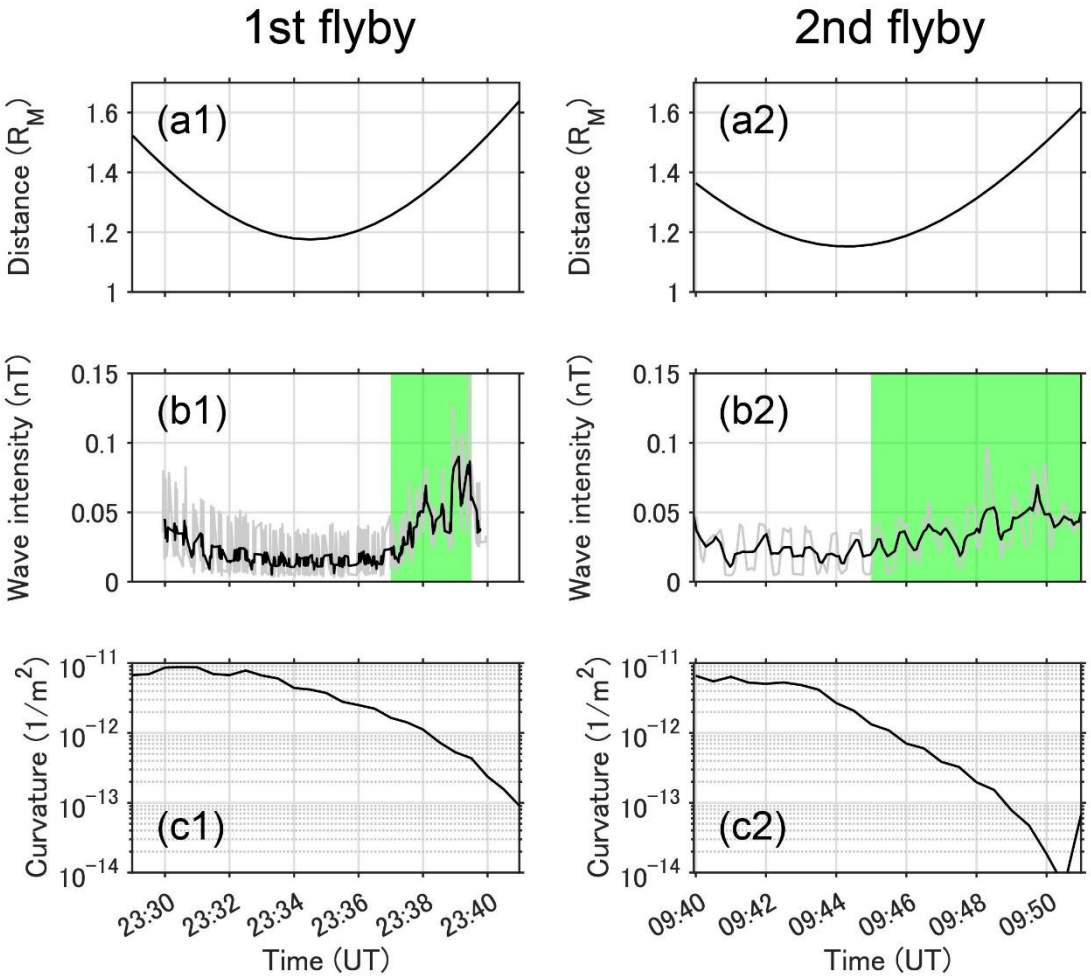

Figure 2. Observed whistler-mode wave intensity related to the distance from Mercury and the background magnetic curvature. (a1 and a2) Distance from Mercury. (b1 and b2) Chorus wave intensity (gray) and smoothed data (black) using a running average. The green areas indicate the observed regions of clear dawn chorus. (c1 and c2) Curvature of the background magnetic field line at the location showing the minimum strength deduced from an empirical model[9].

Simulation results

To numerically estimate the effects of background magnetic field curvature on the generation of chorus emission waves at Mercury, we conducted a one-dimensional full particle-in-cell (PIC) simulation[45] along an ambient background magnetic field line modeled in a Mercury environment (see PIC simulations in Methods). Based on our previous PIC simulation studies, which successfully reconstructed chorus emission waves in the Earth's magnetosphere[36] and revealed the importance of nonlinear resonant currents in the generation of chorus emission waves[42].

We note that the present simulation parameters (see PIC simulations in Methods) are different from the typical values taken for the chorus generation region of the Earth's inner magnetosphere, in particular, we use a 10 times higher density of cold electrons[43], a one-tenth slower velocity of energetic electrons (based on the scaling law[43] and Mariner 10 observations[6]), a 3 times wider loss cone angle at the magnetic equator, and a much larger (10 thousand times) stretching of the background magnetic field line (based on the empirical model[9]). The assumed density ratio of energetic to cold electrons is smaller than that for the Earth's outer magnetosphere (L~10.5)[34]. Therefore, our simulations offer new conditions to study the chorus wave generation, different from those at Earth.

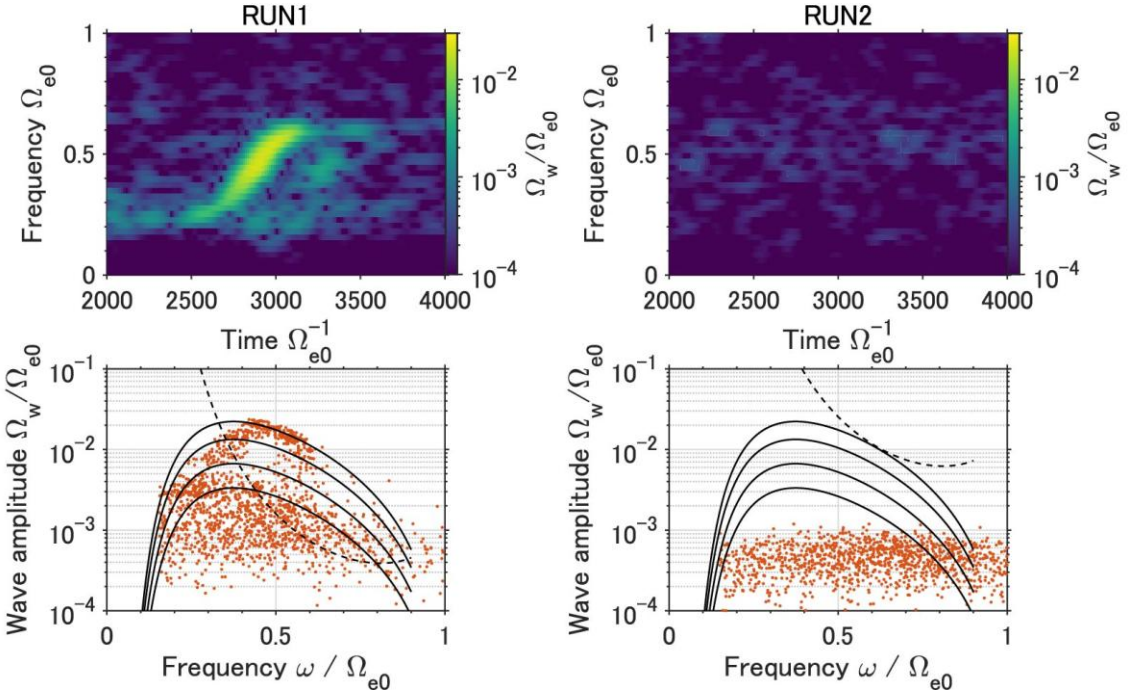

Figure 3. PIC simulations in Mercury's environment. RUN1 is for a less stretched field line condition estimated from the model for flyby observations. RUN2 is for a more stretched field line condition (4 times RUN1). In the lower panels, the black solid curves indicate the optimum amplitudes for $\tau = 0.15, 0.25, 0.5$, and 1.0 from the above curves (see Nonlinear wave growth in Methods section for the definition of τ), the dotted black curves are the threshold amplitude for triggered wave emissions at the source region, and the orange dots are simulated wave amplitudes.

Figure 3 shows simulated dynamic spectra of magnetic field fluctuations of the forward wave packet with two different magnetic inhomogeneities at the magnetic equator: RUN1 has a small magnetic inhomogeneity whose value was determined from the observation conditions using an empirical

magnetic field model[9]; RUN2 has the same setup as RUN1 but with a magnetic inhomogeneity 4-times larger to reflect the conditions in the night sector, thus allowing us to study the impact of the day/night magnetic field asymmetry on the wave generation. In RUN1 we clearly see the rising-tone fine structure of the discrete chorus element similar to Earth's chorus emission waves, but we see no specific wave excitation in RUN2. The spatial development of wave growth in both RUN1 and RUN2 are shown in Supplementary Figures S3 and S4. In the absence of accurate measurements of the cold and energetic electrons densities, it is not possible to compare the wave amplitude observed by Mio with the theoretical amplitude. However, we can compare the chorus amplitudes for the simulation with the theoretical prediction of nonlinear wave growth theory[42] (see Methods). In nonlinear theory, coherent and strong (a few percent of the amplitude of the background magnetic field) chorus emission waves with rising-tone structures can nonlinearly grow from an incoherent seed and weak whistler-mode waves by the effects of a nonlinear resonant current[42]. The triggered condition for the nonlinear wave growth process[42] is given by

$$\frac{\Omega_w}{\Omega_{e0}} > \frac{\Omega_{th}}{\Omega_{e0}},$$

where Ω_w is the wave amplitude, Ω_{th} is the threshold wave amplitude given for the absolute instability, and Ω_{e0} is the electron cyclotron frequency at the magnetic equator (source region). In the nonlinear process, the wave amplitude can take the optimum wave amplitude Ω_{op} for an optimum wave growth condition[42]. The simulated chorus wave amplitudes in RUN1 are consistent with the theoretical optimum amplitudes when the threshold amplitude is lower than the optimum amplitudes. On the other hand, the threshold amplitude in RUN2 is larger than the optimum amplitudes in the whole frequency band. The simulated waves in RUN2 show only thermal and particle noise coming from the limited number of energetic particles in the simulation system, which are not fed by energy transfer from the electrons, and thus did not grow. Therefore, the fine structures of the discrete chorus element observed in the simulation suggest that nonlinear wave-particle energy exchanges can occur under the specific Mercury magnetospheric conditions.

Discussion

Despite operating with a non-deployed boom and limited telemetry in the cruise configuration toward Mercury, the Mio search coil magnetometers of the PWI found dawn chorus waves during the two flybys. This result suggests that chorus emission waves, which control the dynamics of energetic electrons through wave–particle interactions, are ubiquitous in all magnetized planets of our Solar System. The flyby observations strongly support the idea that the background magnetic inhomogeneity has a strong impact on the generation process of planetary chorus waves, which is complemented by the results of simulations in a Mercury environment.

The existence of dawn chorus waves in Mercury suggests the following three-step scenario,

illustrated in Figure 4. (1) The quasi-trapped electron ring current develops a temperature anisotropy, in particular on the dayside, which is the seed for initial whistler-mode wave growth. Mercury's magnetosphere has a larger loss cone angle of approximately 20 to 30 degrees than that of Earth of a few degrees[9]. The effects of drift electron motion in Mercury's complex background magnetic field structures with such large loss cone angles are favorable for the development of temperature anisotropy[41]. Large compressional background magnetic fields in the dayside take bifurcated background magnetic field minima at northward and southward latitudes above the magnetic equator. Then, electrons with high equatorial pitch angles are forced to drift and get reflected at high latitudes without passing through the equatorial plane, the so-called Shabansky orbits[46]. The MESSENGER's plasma observations strongly support the effects of Shabansky orbits in Mercury[16]. These non-energizing (drift shell splitting and Shabansky orbits[41]) processes based on the background magnetic field structures should play a role in developing the temperature anisotropy of seed electrons. (2) Chorus waves strongly and rapidly scatter energetic electrons through wave–particle interactions[47, 48]. The observed dawn chorus waves contribute to electron precipitation on the dawn side, which can generate part of the X-ray aurora observed at Mercury[13, 14]. However, the X-ray aurora for Mercury is widely distributed from midnight to predusk sectors in contrast with the dawn chorus region identified during the 1st and 2nd flybys. A global map of chorus waves in Mercury is important for understanding loss mechanisms of energetic electrons. In particular, the asymmetric loss cone width in the northern and southern hemispheres may influence the northward and southward chorus wave generation. (3) Chorus waves can also rapidly accelerate seed electrons from hundreds of keV to MeV[20, 21, 22, 23, 24] in the limited L-shell. Unlike Earth, Jupiter, and Saturn, Mercury has no permanent electron radiation belt[6, 40]. If a short-duration quasi-trapped radiation belt could be generated at Mercury, chorus waves would play an important role in generating tentative enhancement of higher energy electron populations.

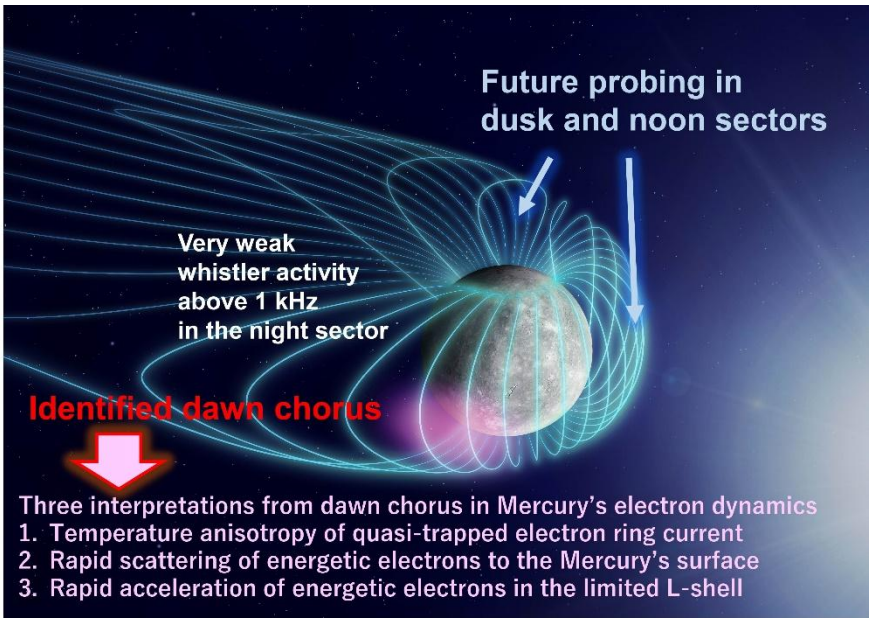

Figure 4. Three possible interpretations deduced from the dawn chorus in Mercury. The map of Mercury is published at https://photojournal.jpl.nasa.gov/catalog/PIA17230. Image credit of Mercury: NASA/Johns Hopkins University Applied Physics Laboratory/Carnegie Institution of Washington.

Further investigations of chorus wave activities are required to better understand the electron dynamics in Mercury. This observational evidence of chorus waves obtained by Mio during its Mercury flybys calls for designing and planning more ambitious scientific observations, even with limited telemetry data, such as probing waveform data during future flybys and the science phase after the final orbit insertion in 2025. The MAST boom on which the search coil sensors are mounted will be fully deployed (up to 5-m length) from the spacecraft body. This deployment will minimize potential electromagnetic interference from the spacecraft, allowing the search coil magnetometers to obtain data with the highest SNR to fully probe the plasma wave environments in Mercury's magnetosphere (including refractive indices, wave-normal angles, polarizations, and fine structures). To date, we still do not know whether the Earth and Mercury have similar spatiotemporal properties of their electron-driven chorus. This question will be investigated by a comparison using new observations of alternating current magnetic fields probed by the search coil magnetometers onboard the Arase satellite at Earth[49] and the Mio spacecraft at Mercury[30]. The present study paves the way for these challenging future investigations that will reveal how magnetized planet environments are shaped by the solar wind in our Solar System, with potential extrapolation to exoplanets and their interactions with stellar winds.

Wave magnetic field measurements

The wave magnetic field signals measured by the search coil magnetometers[30] are processed by plasma wave instruments (PWI)[29] and the VLF wave spectrum is covered by the onboard frequency analyzer (OFA) of the PWI. In the 1st Mercury flyby, we took a higher temporal resolution of 1 s using relatively few frequency bins of only 90 points from 32 Hz to 1.8 kHz in a linear increase of a 32-Hz bandwidth and from 1.8 kHz to 20 kHz in a logarithmically increasing bandwidth. In the 2nd Mercury flyby, we used a lower temporal resolution of 4 s and a higher frequency resolution with 360 points for 32 Hz to 10 kHz in a linear increase and 10 kHz to 20 kHz in a logarithmic increase. In both flybys, only wave spectra were measured (no waveforms) because of the limited telemetry data in the cruise phase during which the spacecraft is not spinning.

Unfortunately, the wave magnetic field below 1 kHz was contaminated by electromagnetic interference, though this will be reduced after the separation of Mio from the cruise module after Mercury orbital insertion. Figures 1, 2, and S1 are plotted using the square root of the intensity by the beta-axial sensor of the low frequency search coil (LF-SC) and the gamma-axial sensor of the dual-band search coil (DBSC) mounted on the top plate. The raw wave magnetic field spectra that include some noise are shown in Figure S1 in SI. The denoised wave spectra are shown in Figure 1 to provide further details on the whistler-mode waves. The line spectra showing the 1st to 10th maximum power were suppressed during the denoising process. The noise-equivalent magnetic induction (NEMI) for the LF-SC is approximately 40 fT/Hz$^{1/2}$ and the NEMI for DBSC is 60 fT/Hz$^{1/2}$ at a frequency of 1 kHz[30], which are sufficiently low for probing the observed whistler-mode waves showing pT-intensity levels. In Figure 2, the wave magnetic field intensity is calculated by integrating the raw spectrum in the frequency range from $0.2f_{\mathrm{ce}}$ to $0.75f_{\mathrm{ce}}$ for the 1st flyby and from $0.2f_{\mathrm{ce}}$ to $0.45f_{\mathrm{ce}}$ for the 2nd flyby for a typical frequency range of chorus emission waves, where f_{ce} is the local cyclotron frequency calculated from an empirical model[9]. We considered a narrower integration bandwidth during the 2nd flyby because the wave data is subject to stronger interference. If the value of $0.2f_{\mathrm{ce}}$ is lower than 500 Hz, the wave magnetic field intensities were not calculated to avoid noise contamination. The characteristics of the magnetic field curvature in Figure 2 did not change when using a different value of $s = 0.4\mathrm{R_M}$.

PIC simulations

We model the dawn chorus in Mercury by flyby events using fully kinetic PIC code, which self-consistently solves Maxwell's equations and equations of particle motion taking into account the nonlinear Lorentz force and the mirror force coming from the background magnetic inhomogeneity. The simulation focuses on the region near the magnetic equator, which gives the maximum linear wave growth[36]. The physical spatial scale is $\pm 10.24\ c/\Omega_{\mathrm{e0}}$ centered on the magnetic equator. The cell size satisfies the Courant condition[42]. To evaluate the generation process for chorus emission

waves in the stretched Mercury background magnetic inhomogeneity and prevent nonphysical diffusion by enhanced electrostatic thermal fluctuations, we neglect the parallel electric field with respect to the background field line and the difference in the loss-cone width for both the northern and southern hemispheres. The background magnetic field line is simply modeled as a parabolic function as written in Equation 1 ($a = 2.4 \times 10^{-3}\ c^{-2}\Omega_{e0}^2$ for RUN1) and the loss-cone size at the magnetic equator is 15.5 degrees. Hot electrons in Mercury's plasma sheet were identified using in-situ observations of Mariner 10[6]. Electron density in Mercury's magnetosphere were of the order of 5 particles/cm3 on an average and the typical energies ranged from 0.1 to 1 keV based on the Mariner 10 electron measurements. A part of these hot plasma sheet electrons with a temperature anisotropy should become a source to excite initial whistler-mode waves. The Mariner 10 electron measurements revealed the presence of cold and dense plasma sheet and also hot and tenuous plasm sheet with a rapid change. The plasma mass density was found to vary from 1 to 650 amu/cm3 using field line resonance by MESSENGER magnetometer data[50]. We simply use two populations of electrons in the simulation: a cold population described by an isotropic Maxwellian distribution and an energetic population obeying an anisotropic Maxwellian distribution with a loss cone. We set the initial perpendicular and parallel velocity components (with respect to the background magnetic field) to $V_{\mathrm{th}\perp} = 0.079c$ and $V_{\mathrm{th}\parallel} = 0.053c$, where c is the speed of light. We further assume background immobile ions to neutralize the total plasma electric charge. In the linear wave growth phase, as the temperature anisotropy of energetic electrons is an important parameter, we assume a weak temperature anisotropy $A_T = \frac{T_\perp}{T_{||}} - 1 = 1.2$, where $T_\perp$ and $T_{||}$ are electron temperatures perpendicular and parallel to the field line. Typical temperature and densities of both cold and energetic electrons for Mercury are determined from a scaling law between the Earth's plasma sheet and the solar wind[43]. The density ratio of energetic to cold electrons is 0.05 and the ratio of plasma and cyclotron frequencies is 12. We assumed a severe condition using a dense cold component because the wave growth rate depends on the density ratio of energetic to cold electrons[36] and can take a larger value in a case with a hot and tenuous plasm sheet where the density ratio can be relatively high.

Nonlinear wave growth

The threshold and optimum wave amplitudes are written as[42]

$$\frac{\Omega_{\mathrm{th}}}{\Omega_{\mathrm{e0}}} = \frac{100\pi^3\gamma^4\xi}{\tilde{\omega}\tilde{\omega}_{\mathrm{ph}}^4(\chi\tilde{U}_{\perp 0})^5}\left(\frac{\tilde{a}s_2\tilde{U}_{t\parallel}}{Q}\right)^2 \exp\left(\frac{\gamma^2\tilde{V}_{\mathrm{R}}^2}{\tilde{U}_{t\parallel}^2}\right)$$

and

$$\frac{\Omega_{\mathrm{op}}}{\Omega_{\mathrm{e0}}} = 0.8\pi^{-5/2}\frac{|Q|\tilde{V}_{\mathrm{p}}\tilde{V}_{\mathrm{g}}}{\tau\tilde{\omega}}\frac{\tilde{U}_{\perp 0}}{\tilde{U}_{t\parallel}}\tilde{\omega}_{\mathrm{ph}}^2\left(1-\frac{\tilde{V}_{\mathrm{R}}}{\tilde{V}_{\mathrm{g}}}\right)^2 \exp\left(-\frac{\gamma^2\tilde{V}_{\mathrm{R}}^2}{2\tilde{U}_{t\parallel}^2}\right),$$

where the symbol "~" indicates normalized parameters (i.e., $\tilde{V}_\mathrm{p} = V_\mathrm{P}/c$, $\tilde{V}_\mathrm{g} = V_\mathrm{g}/c$, $\tilde{V}_\mathrm{R} = V_\mathrm{R}/c$, $\tilde{\omega} = \omega/\Omega_{\mathrm{e}0}$, $\tilde{\omega}_\mathrm{ph} = \omega_\mathrm{ph}/\Omega_{\mathrm{e}0}$, $\tilde{U}_{\perp 0} = U_{\perp 0}/c$, $\tilde{U}_{t\parallel} = U_{t\parallel}/c$, $\tilde{a} = ac^2/\Omega_{\mathrm{e}0}^2$),
a is the coefficient of background magnetic field inhomogeneity at the generation region (magnetic equator),
Q is the depth of an electron hole,
γ is the Lorentz factor,
τ is the ratio of the nonlinear trapping time to the nonlinear transition time,
$\xi^2 = \omega(\Omega_\mathrm{e} - \omega)/\omega_\mathrm{pe}^2$ is a dimensionless parameter,
$\chi^2 = (1 + \xi^2)^{-1}$ is a dimensionless parameter,
ω is the wave frequency,
ω_pe is the plasma frequency for background cold electrons,
ω_ph is the plasma frequency for energetic electrons,
Ω_e is the electron cyclotron frequency,
V_P is the phase velocity,
V_g is the group velocity,
V_R is the resonance velocity,
$U_{\perp 0}$ is the average perpendicular momentum of energetic electrons, and
$U_{t\parallel}$ is the thermal momentum in the parallel direction. All parameters except for Q and τ are determined from the initial conditions in the PIC simulations. In Figure 3, the value of Q is assumed to be 0.5 since this is a typical value.

Data availability

The spacecraft orbit data is available from SPICE data for BepiColombo https://www.cosmos.esa.int/web/spice/spice-for-bepicolombo. The PWI data will be available from the Center for Heliospheric Science https://chs.isee.nagoya-u.ac.jp/en/, or from the corresponding author upon reasonable request.

Code availability

The PIC simulations are based on the literatures[36, 42] and the PIC code (KEMPO1) is available at http://space.rish.kyoto-u.ac.jp/software/.

References (<= 50)

1. Baumjohann, W., Blanc, M., Fedorov, A. et al. Current Systems in Planetary Magnetospheres

and Ionospheres. Space Science Reviews, 152, 99–134 (2010). https://doi.org/10.1007/s11214-010-9629-z

2. Tsurutani, B. T., Lakhina, G. S., Sen, A., Hellinger, P., Glassmeier, K.-H. & Mannucci, A. J. A review of Alfvénic turbulence in high-speed solar wind streams: Hints from cometary plasma turbulence. Journal of Geophysical Research: Space Physics, 123, 2458– 2492. (2018). https://doi.org/10.1002/2017JA024203
3. Baker, D., Jaynes, A., Hoxie, V. et al. An impenetrable barrier to ultrarelativistic electrons in the Van Allen radiation belts. Nature, 515, 531–534 (2014). https://doi.org/10.1038/nature13956
4. Domingue, D.L., Koehn, P.L., Killen, R.M. et al. Mercury's Atmosphere: A Surface-Bounded Exosphere. Space Science Reviews, 131, 161–186 (2007). https://doi.org/10.1007/s11214-007-9260-9
5. Ness, N. F., K. W. Behannon, R. P. Lepping, Y. C. Whang, and K. H. Schatten. Magnetic field observations near Mercury: Preliminary results from Mariner 10, Science, 185 (4146), 151–160, (1974). doi:10.1126/science.185.4146.151.
6. Ogilvie, K. W., Scudder, J. D., Vasyliunas, V. M., Hartle, R. E., & Siscoe, G. L. (1977). Observations at the planet Mercury by the Plasma Electron Experiment: Mariner 10. Journal of Geophysical Research, 82(13), 1807– 1824. https://doi.org/10.1029/JA082i013p01807.
7. Anderson, B. J. et al. The global magnetic field of mercury from MESSENGER orbital observations. Science, 333, 1859 (2011).
8. Anderson, B. J., Johnson, C. L., and Korth, H. A magnetic disturbance index for Mercury's magnetic field derived from MESSENGER Magnetometer data, Geochem. Geophys. Geosyst., 14, 3875– 3886, (2013). doi:10.1002/ggge.20242
9. Korth, H., Johnson, C. L., Philpott, L., Tsyganenko, N. A., & Anderson, B. J. A dynamic model of Mercury's magnetospheric magnetic field. Geophysical Research Letters, 44, 10,147– 10,154. (2017). https://doi.org/10.1002/2017GL074699
10. Zhao, JT., Zong, QG., Yue, C. et al. Observational evidence of ring current in the magnetosphere of Mercury. Nature Communications, 13, 924 (2022). https://doi.org/10.1038/s41467-022-28521-3
11. Baker, D. N., et al. Intense energetic electron flux enhancements in Mercury's magnetosphere: An integrated view with high-resolution observations from MESSENGER, Journal of Geophysical Research: Space Physics, 121, 2171– 2184, (2016). doi:10.1002/2015JA021778.
12. Ho, G. C., Starr, R. D., Krimigis, S. M., Vandegriff, J. D., Baker, D. N., Gold, R. E., Anderson, B. J., Korth, H., Schriver, D., Jr. McNutt, R. L., et al. MESSENGER observations of suprathermal electrons in Mercury's magnetosphere, Geophysical Research Letters, 43, 550–555, (2016). doi:10.1002/2015GL066850.
13. Lindsay, S.T., James, M.K., Bunce, E.J., Imber, S.M., Korth, H., Martindale, A., Yeoman, T.K.,

MESSENGER X-ray observations of magnetosphere–surface interaction on the nightside of Mercury, Planetary and Space Science, 125, 72-79, (2016). https://doi.org/10.1016/j.pss.2016.03.005.

14. Lindsay, S. T., Bunce, E. J., Imber, S. M., Martindale, A., Nittler, L. R., & Yeoman, T. K. MESSENGER X-ray observations of electron precipitation on the dayside of Mercury. Journal of Geophysical Research: Space Physics, 127, e2021JA029675. (2022). https://doi.org/10.1029/2021JA029675
15. Slavin, J.A., Imber, S.M. and Raines, J.M. (2021). A Dungey Cycle in the Life of Mercury's Magnetosphere. In Magnetospheres in the Solar System (eds R. Maggiolo, N. André, H. Hasegawa, D.T. Welling, Y. Zhang and L.J. Paxton). https://doi.org/10.1002/9781119815624.ch34
16. Dewey, R. M., Slavin, J. A., Raines, J. M., Baker, D. N., & Lawrence, D. J. (2017). Energetic electron acceleration and injection during dipolarization events in Mercury's magnetotail. Journal of Geophysical Research: Space Physics, 122, 12,170– 12,188. https://doi.org/10.1002/2017JA024617
17. Burton, R. K., and Holzer, R. E. The origin and propagation of chorus in the outer magnetosphere, Journal of Geophysical Research, 79(7), 1014– 1023, (1974). doi:10.1029/JA079i007p01014.
18. Tsurutani, B. T., and Smith, E. J. Postmidnight chorus: A substorm phenomenon, Journal of Geophysical Research, 79(1), 118– 127, (1974). doi:10.1029/JA079i001p00118.
19. Summers, D., Thorne, R. M., and Xiao, F. Relativistic theory of wave-particle resonant diffusion with application to electron acceleration in the magnetosphere, Journal of Geophysical Research, 103(A9), 20487– 20500, (1998). doi:10.1029/98JA01740.
20. Thorne, R., Li, W., Ni, B. et al. Rapid local acceleration of relativistic radiation-belt electrons by magnetospheric chorus. Nature, 504, 411–414 (2013). https://doi.org/10.1038/nature12889
21. Horne, R., Thorne, R., Glauert, S. et al. Gyro-resonant electron acceleration at Jupiter. Nature Physics, 4, 301–304 (2008). https://doi.org/10.1038/nphys897
22. Woodfield, E. E., Glauert, S. A., Menietti, J. D., Averkamp, T. F., Horne, R. B., & Shprits, Y. Y. Rapid electron acceleration in low-density regions of Saturn's radiation belt by whistler mode chorus waves. Geophysical Research Letters, 46, 7191– 7198. (2019). https://doi.org/10.1029/2019GL083071
23. Omura, Y., Miyashita, Y., Yoshikawa, M., Summers, D., Hikishima, M., Ebihara, Y., and Kubota, Y. Formation process of relativistic electron flux through interaction with chorus emissions in the Earth's inner magnetosphere, Journal of Geophysical Research: Space Physics, 120, 9545– 9562, (2015). doi:10.1002/2015JA021563.
24. Allison, H. J., Shprits, Y. Y., Zhelavskaya, I. S., Wang, D. & Smirnov, A. G. Gyroresonant

wave-particle interactions with chorus waves during extreme depletions of plasma density in the Van Allen radiation belts, Science Advances, 7, (2021). DOI: 10.1126/sciadv.abc0380

25. Kurth, W. S., and Gurnett, D. A. Plasma waves in planetary magnetospheres, Journal of Geophysical Research, 96(S01), 18977– 18991, (1991). doi:10.1029/91JA01819.
26. Milillo, A., Fujimoto, M., Murakami, G. et al. Investigating Mercury's Environment with the Two-Spacecraft BepiColombo Mission. Space Science Reviews, 216, 93 (2020). https://doi.org/10.1007/s11214-020-00712-8
27. Benkhoff, J., Murakami, G., Baumjohann, W. et al. BepiColombo - Mission Overview and Science Goals. Space Science Reviews, 217, 90 (2021). https://doi.org/10.1007/s11214-021-00861-4
28. Saito, Y., Delcourt, D., Hirahara, M. et al. Pre-flight Calibration and Near-Earth Commissioning Results of the Mercury Plasma Particle Experiment (MPPE) Onboard MMO (Mio). Space Science Reviews, 217, 70 (2021). https://doi.org/10.1007/s11214-021-00839-2
29. Kasaba, Y., Kojima, H., Moncuquet, M. et al. Plasma Wave Investigation (PWI) Aboard BepiColombo Mio on the Trip to the First Measurement of Electric Fields, Electromagnetic Waves, and Radio Waves Around Mercury. Space Science Reviews, 216, 65 (2020). https://doi.org/10.1007/s11214-020-00692-9
30. Yagitani, S., Ozaki, M., Sahraoui, F. et al. Measurements of Magnetic Field Fluctuations for Plasma Wave Investigation by the Search Coil Magnetometers (SCM) Onboard Bepicolombo Mio (Mercury Magnetospheric Orbiter). Space Science Reviews, 216, 111 (2020). https://doi.org/10.1007/s11214-020-00734-2
31. Li, W., Thorne, R. M., Angelopoulos, V., Bortnik, J., Cully, C. M., Ni, B., LeContel, O., Roux, A., Auster, U., and Magnes, W. Global distribution of whistler-mode chorus waves observed on the THEMIS spacecraft, Geophys. Res. Lett., 36, L09104, (2009). doi:10.1029/2009GL037595.
32. Meredith, N. P., Horne, R. B., Shen, X.-C., Li, W., & Bortnik, J. Global model of whistler mode chorus in the near-equatorial region ($|\lambda m| < 18°$). Geophysical Research Letters, 47, e2020GL087311. (2020). https://doi.org/10.1029/2020GL087311
33. Burtis, W. J. & Helliwell, R. A. Banded chorus—A new type of VLF radiation observed in the magnetosphere by OGO 1 and OGO 3. Journal of Geophysical Research, 74, 3002–3010 (1969).
34. Yagitani, S., Habagishi, T., and Omura, Y. Geotail observation of upper band and lower band chorus elements in the outer magnetosphere, Journal of Geophysical Research: Space Physics, 119, 4694– 4705, (2014). doi:10.1002/2013JA019678.
35. Li, J., Bortnik, J., An, X. et al. Origin of two-band chorus in the radiation belt of Earth. Nature Communications, 10, 4672 (2019). https://doi.org/10.1038/s41467-019-12561-3
36. Hikishima, M., Yagitani, S., Omura, Y., and Nagano, I. Full particle simulation of

whistler-mode rising chorus emissions in the magnetosphere, Journal of Geophysical Research, 114, A01203, (2009). doi:10.1029/2008JA013625.

37. Ebihara, Y., Ikeda, T., Omura, Y., Tanaka, T., & Fok, M.-C. Nonlinear wave growth analysis of whistler-mode chorus generation regions based on coupled MHD and advection simulation of the inner magnetosphere. Journal of Geophysical Research: Space Physics, 125, e2019JA026951. (2020). https://doi.org/10.1029/2019JA026951
38. Katoh, Y., and Omura, Y. Effect of the background magnetic field inhomogeneity on generation processes of whistler-mode chorus and broadband hiss-like emissions, Journal of Geophysical Research: Space Physics, 118, 4189– 4198, (2013). doi:10.1002/jgra.50395.
39. Wu, Y., Tao, X., Zonca, F., Chen, L., & Wang, S. Controlling the chirping of chorus waves via magnetic field inhomogeneity. Geophysical Research Letters, 47, e2020GL087791. (2020). https://doi.org/10.1029/2020GL087791
40. Schriver, D., et al. Quasi-trapped ion and electron populations at Mercury, Geophysical Research Letters, 38, L23103, (2011). doi:10.1029/2011GL049629.
41. Walsh, B. M., Ryou, A. S., Sibeck, D. G., and Alexeev, I. I. Energetic particle dynamics in Mercury's magnetosphere, Journal of Geophysical Research: Space Physics, 118, 1992– 1999, (2013). doi:10.1002/jgra.50266.
42. Omura, Y. Nonlinear wave growth theory of whistler-mode chorus and hiss emissions in the magnetosphere. Earth Planets Space, 73, 95 (2021). https://doi.org/10.1186/s40623-021-01380-w
43. Mukai, T., Ogasawara, K., & Saito, Y., An empirical model of the plasma environment around Mercury, Advances in Space Research, 33(12), 2166-2171, (2004). https://doi.org/10.1016/S0273-1177(03)00443-5.
44. Kennel, C. F., and Petschek, H. E. Limit on stably trapped particle fluxes, Journal of Geophysical Research, 71(1), 1– 28, (1966). doi:10.1029/JZ071i001p00001.
45. Omura, Y., One-dimensional electromagnetic particle code: KEMPO1, in Advanced Methods for Space Simulations, edited by H. Usui and Y. Omura, pp. 1 – 21, (2007). Terra Sci., Tokyo.
46. McCollough, J. P., Elkington, S. R., and Baker, D. N. The role of Shabansky orbits in compression-related electromagnetic ion cyclotron wave growth, Journal of Geophysical Research, 117, A01208, (2012). doi:10.1029/2011JA016948.
47. Ozaki, M., Miyoshi, Y., Shiokawa, K. et al. Visualization of rapid electron precipitation via chorus element wave–particle interactions. Nature Communications 10, 257 (2019). https://doi.org/10.1038/s41467-018-07996-z
48. Hsieh, Y.-K., Omura, Y., & Kubota, Y. Energetic electron precipitation induced by oblique whistler mode chorus emissions. Journal of Geophysical Research: Space Physics, 127, e2021JA029583. (2022). https://doi.org/10.1029/2021JA029583

49. Ozaki, M., Yagitani, S., Kasahara, Y. et al. Magnetic Search Coil (MSC) of Plasma Wave Experiment (PWE) aboard the Arase (ERG) satellite. Earth Planets Space 70, 76 (2018). https://doi.org/10.1186/s40623-018-0837-1
50. James, M. K., Imber, S. M., Yeoman, T. K., & Bunce, E. J. Field line resonance in the Hermean magnetosphere: Structure and implications for plasma distribution. Journal of Geophysical Research: Space Physics, 124, 211– 228. (2019). https://doi.org/10.1029/2018JA025920

Acknowledgements

The authors would like to express their sincere thanks to all the Mio and BepiColombo project members for their careful contributions to the projects' operations. The Japanese authors express their deep appreciation to Dr. Hiroshi Matsumoto, Dr. Isamu Nagano, Dr. Hirotsugu Kojima, and Dr. Hajime Hayakawa for their valuable comments during the development of the PWI. The present study was supported in part by the JSPS, KAKENHI grant JP20H02162. This paper is based on observations obtained with BepiColombo, a joint ESA - JAXA science mission with instruments and contributions directly funded by ESA Member States and JAXA.

Author contributions

M.O. developed the scientific content of the study, analyzed the search coil data, numerically computed the chorus waves modeled in Mercury's environment, wrote this manuscript, produced the figures, and contributed to the development of the LF-SC of the PWI. S.Y. led the development of the LF-SC of the PWI and contributed to the PWI data analysis. Y.Kasaba is the principal investigator of the PWI and led the PWI observations during the flybys. Y.Kasahara and S.M. contributed to the PWI data production and analysis. Y.O. and M.H. contributed to the PIC simulations, the numerical analysis based on the nonlinear wave growth theory, and its interpretation. S.K is a member of BepiColombo young scientist group and contributed to the PWI data analysis. F.S., L.M., and G.C. contributed to the evaluation of the DBSC data, its interpretation, and editing of the manuscript. S.N. led the electromagnetic compatibility assessments of the Mio spacecraft and contributed to the improvement of the PWI data by removing spacecraft noise. G.M. is the project scientist and contributed to the Mercury flyby operations. All the authors provided feedback on the manuscript.

Competing interests

The authors declare no competing interests.